New Journal of Physics
The open access journal at the forefront of physics

PAPER • OPEN ACCESS

Erasing Doppler dephasing error in Rydberg quantum gates

To cite this article: Rui Li *et al* 2025 *New J. Phys.* **27** 054502

View the article online for updates and enhancements.

IOP Publishing New J. Phys. 27 (2025) 054502 https://doi.org/10.1088/1367-2630/adcfbe

New Journal of Physics
The open access journal at the forefront of physics

Deutsche Physikalische Gesellschaft DPG
IOP Institute of Physics

Published in partnership with: Deutsche Physikalische Gesellschaft and the Institute of Physics

OPEN ACCESS

RECEIVED
24 January 2025

REVISED
3 April 2025

ACCEPTED FOR PUBLICATION
23 April 2025

PUBLISHED
6 May 2025

PAPER

Erasing Doppler dephasing error in Rydberg quantum gates

Rui Li[1], **Jing Qian**[3,4,5,6,*] **and Weiping Zhang**[1,2,5,6,7]

[1] School of Physics and Astronomy, Shanghai Jiao Tong University, Shanghai, 200240, People's Republic of China
[2] Tsung-Dao Lee Institute, Shanghai Jiao Tong University, Shanghai, 200240, People's Republic of China
[3] Department of Physics, School of Physics and Electronic Science, East China Normal University, Shanghai, 200062, People's Republic of China
[4] Chongqing Institute of East China Normal University, Chongqing 401120, People's Republic of China
[5] Shanghai Research Center for Quantum Science, Shanghai 201315, People's Republic of China
[6] Shanghai Branch, Hefei National Laboratory, Shanghai 201315, People's Republic of China
[7] Collaborative Innovation Center of Extreme Optics, Shanxi University, Taiyuan, Shanxi 030006, People's Republic of China
[*] Author to whom any correspondence should be addressed.

E-mail: jqian1982@gmail.com

Keywords: Doppler dephasing error, quantum gates, Rydberg atoms, optimal control

Abstract

The Doppler dephasing error due to residual thermal motion of atoms is a major cause of infidelity in neutral-atom quantum gates. Besides cooling and trapping advancements, few effective methods exist to mitigate this error. In the present work, we first propose an error-erasing strategy that utilizes a pair of off-resonant fields to continuously dress the protected Rydberg state with an auxiliary state, which can induce an opposite but enhanced sensitivity to the same source of Doppler dephasing error. Combining with the optimal control of laser pulses, we have realized a family of Rydberg two-qubit controlled-NOT gates in Rb and Cs atoms that are fully immune to the Doppler dephasing error. We numerically simulate this gate operation with fidelity $F \approx 0.9906$ at *any* temperature for a lower-excited auxiliary state, and a higher fidelity of $F \approx 0.9960$ can be attained for a ground auxiliary state even at a temperature of 500 μK. Finally, we predict a super-high fidelity of $F > 0.9999$ for 50 μK is possible by using the robust pulses with a larger amplitude. Our results significantly reduce atomic temperature requirements for high-fidelity quantum gates, and may provide fundamental guidance to practical fault-tolerant quantum computing with neutral atoms.

1. Introduction

Errors restrict the fidelity of Rydberg gates in neutral-atom quantum computing and must be made sufficiently low by using versatile fault-tolerant techniques [1–6]. So far, the ability to reduce the sensitivity of gate operations to various intrinsic and technical errors by using robust pulses is a key capability for constructing a neutral-atom quantum computer [7, 8], and the best reported fidelity for a two-qubit controlled-phase gate has reached 0.995 relying on optimal control strategy [9]. Typically, a simple time-optimal gate with robust pulses only maximizes the ideal gate fidelity in the absence of any error yet it can be substantially impacted if the type of errors occurs [10, 11]. Recent efforts have shown that gate protocols can be made natively robust to certain error sources either by modifying the cost function in optimization [12–17] or by converting the feature of quasistatic errors [18]. However, to further improve the robustness of gates against certain type of errors beyond pure numerical methods, remains a great challenge.

As we know, decoherence from residual atomic motion fundamentally limits the gate fidelity in experiments [19, 20]. Atoms, whether they are warm or cold, are not stationary, inevitably leading to the motional dephasing due to inhomogeneous velocity distribution. Although a traditional two-photon transition with two counterpropagating excitation lasers can diminish the impact of Doppler dephasing, nevertheless, this improvement is very limited in a sense [21–25] except for using more technically demanding three-photon excitation where the overall Doppler effect turns to be exactly zero based on the starlike planar geometry [26]. Therefore, such a Doppler dephasing error remains a crucial resource of technical errors for promising applications in quantum information processing. However, it is rarely mitigated unless actual colder temperatures $\sim\mu$K are reached [27, 28]. With the recent demonstration of a coherence protection scheme in thermal atomic ensembles by Finkelstein *et al* [29], where a collective state can be fully protected from inhomogeneous dephasing by employing off-resonant fields that dress it to an auxiliary sensor state (note that this scheme has also been implemented to quantum memories with improved performance [30]), there is a significant interest in achieving a Doppler-error erased gate by applying this scheme.

In this work, we introduce a family of erasure protocols for realizing two-qubit Rydberg controlled-NOT (CNOT) gates, which exhibit full robustness to the Doppler dephasing error originating from the thermal motion of atoms. In combination with the optimal control method [31–33], our novel protocols employ a pair of off-resonant laser fields continuously dressing the protected Rydberg state with a lower-excited auxiliary state that has an opposite but enhanced sensitivity to the same error source. The resulting gates have shown an absolute immunity to the Doppler dephasing error impacted on the Rydberg level at *any* temperature. All gate pulses including their amplitudes and phases as well as the gate duration are globally optimized, avoiding the requirement for stepwise operations [34, 35].

To characterize the compatibility of our protocol to various atomic systems, we explore the results using different dressing cases in Rb and Cs atoms and show the choice of a higher sensitivity factor is key to improve the gate performance. We analyze the method to suppress spontaneous decay errors from the auxiliary excited state which ultimately limits the gate fidelity presently [36]. Furthermore, we instead utilize a ground-state auxiliary state for avoiding the inherent decay error and identify the realization of two-qubit CNOT gates with 0.9960 fidelity at $T = 500\,\mu$K yet sacrificing a slight insensitivity to the Doppler shifts because of an unprotected Rydberg state. Besides, by enhancing the limitation for maximal laser amplitude to be $2\pi\times 20$ MHz, we find the predicted fidelity number can even be above 0.9999 attributing to the strong suppression of intermediate time-spent. Finally, with the increase of finite temperature of atoms, we confirm that the newly-proposed dressing protocols are significantly superior to the typical two-photon excitation gates, by mutually having a higher fidelity and a lower Doppler dephasing error over a very wide range of atomic temperatures.

2. Model and Hamiltonians

To implement the Doppler dephasing-error erased gate, we assume the level scheme as shown in figure 1. Each atom is modeled as a four-level system with long-lived ground states $|0\rangle, |1\rangle$, an uppermost Rydberg state $|r\rangle$ with lifetime $1/\tau_r$ and a lower-excited auxiliary state $|e\rangle$ with lifetime $1/\tau_e$. The traditional coupling between $|1\rangle$ and $|r\rangle$ is enabled by a global two-photon laser pulse with time-dependent Rabi frequency $\Omega_\mathrm{r}(t)$, between $|0\rangle$ and $|r\rangle$ by $\Omega_\mathrm{r}'(t)$. Moreover, the laser frequency is tuned to be resonant with the transition between $|1\rangle$ (or $|0\rangle$) and $|r\rangle$. Additionally, we require a pair of dressing fields off-resonantly coupling $|r\rangle$ and $|e\rangle$ with a same strength Ω_d and opposite detunings $\Delta_\mathrm{d}, -\Delta_\mathrm{d}$, possibly generated by using an electro-optic modulator [29]. As a consequence, when the Doppler effect causes an uncertain detuning error of $|1\rangle\to|r\rangle$ transition, i.e. $-\delta = \vec{k}_r\cdot\vec{v}$, state $|e\rangle$ can also be affected by the same source of inhomogeneity from same atomic velocity, experiencing an unknown energy shift $\chi\delta = (\vec{k}_r+\vec{k}_a)\cdot\vec{v}$ with $\chi = |1+\vec{k}_a/\vec{k}_r|$. Here, the opposite sign $(-\delta,\chi\delta)$ is ensured by the choice of different wavevectors of lasers $(\vec{k}_a,\vec{k}_r)$ as well as their propagation directions. For simplicity, the two-photon transition on the target qubit driving $|0\rangle$ and $|r\rangle$ is enabled by a same wavevector $\vec{k}_r$.

We require the sensitivity factor to be $\chi\geqslant 1$, which means the dressing state $|e\rangle$ senses the fluctuation at least as comparable as the Rydberg state $|r\rangle$. This process can be achieved by an optical transition whose wavevector $\vec{k}_a$ has an opposite direction yet a much larger magnitude (i.e. a shorter wavelength). In two-photon transitions, the excitation wavevector $\vec{k}_r$ is a vectorial sum of participating fields' wavevectors. Their intermediate state $|e'\rangle$ (not shown, we choose $|e'\rangle = |5P_{3/2}\rangle$) and dressing state $|e\rangle$ determines the ratio $\vec{k}_a/\vec{k}_r$. Note that the transition $|r\rangle\to|e\rangle$ should have an enhanced and opposite velocity sensitivity as compared to that of $|1\rangle\to|r\rangle$, consequently the choice of $|e\rangle$ is vital. A nearby long-lived Rydberg state is impossible to be $|e\rangle$. Thereby, we first suggest protecting the Rydberg state $|r\rangle = |70S_{1/2}\rangle$ by dressing it to a lower excited state $|e\rangle = |5P_{1/2}\rangle$ in ^{87}Rb atoms. This choice provides $\vec{k}_r = 2\pi(\lambda_{480}^{-1}-\lambda_{780}^{-1}) = 5.035\,\mu m^{-1}$, $\vec{k}_a = -2\pi/\lambda_{475} = -13.228\,\mu m^{-1}$, arising the sensitivity factor $\chi\approx 1.627$ if $\Omega_\mathrm{d}/\Delta_\mathrm{d}\approx 0.698$. Note that, in order to improve the practical relevance, in section 6 we alternatively introduce $|e\rangle$ to be a hyperfine ground state where the one-photon transition between the Rydberg and auxiliary states is performed by an ultraviolet laser [37]. This choice could entirely avoid the spontaneous decay from $|e\rangle$ and make the scheme benefited from a higher fidelity at lower temperatures.

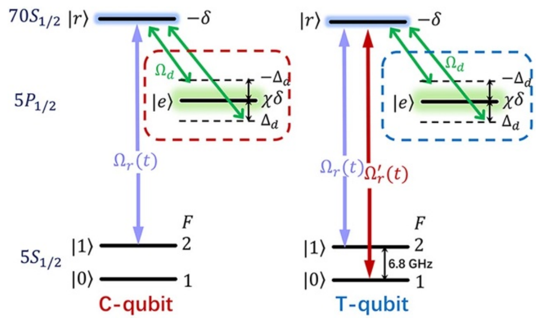

Figure 1. Doppler dephasing error erased two-qubit CNOT gates. Level scheme: qubit states $|0\rangle, |1\rangle$ are encoded in hyperfine clock states $|5S_{1/2}, F=1, m_F=0\rangle$ and $|5S_{1/2}, F=2, m_F=0\rangle$ of two ^{87}Rb atoms. The $|0\rangle$ and $|1\rangle$ states are coupled to the Rydberg state $|r\rangle$ with two-photon Rabi frequency of real amplitudes $\Omega_\mathrm{r}, \Omega_\mathrm{r}'$ and phases ϕ, ϕ', which undergo an unknown Doppler shift $-\delta$ due to the atomic velocity. Additionally, two dressing fields with the same Rabi frequency Ω_d and opposite detunings $\Delta_\mathrm{d}, -\Delta_\mathrm{d}$ enable the coupling between $|r\rangle$ and a lower-excited auxiliary state $|e\rangle$ (here $|e\rangle = |5P_{1/2}\rangle$). The overall transition frequency between $|1\rangle$ and $|e\rangle$ will experience an energy shift $\chi\delta$, possibly opposite and larger as required by the insensitive condition (see appendix A). The intrinsic error treating as the ultimate limit for the gate fidelity is the spontaneous decay from state $|e\rangle$ (see section 5.2).

The total Hamiltonian governing the dynamics of two atoms reads

$$\mathcal{H} = \mathcal{H}_c \otimes I + I \otimes \mathcal{H}_t + V|rr\rangle\langle rr| \tag{1}$$

with single-qubit Hamiltonians

$$\mathcal{H}_c = \frac{\Omega_\mathrm{r}(t)}{2}|1\rangle\langle r| + \frac{\Omega_\mathrm{d}\left(\mathrm{e}^{\mathrm{i}\Delta_\mathrm{d}t} + \mathrm{e}^{-\mathrm{i}\Delta_\mathrm{d}t}\right)}{2}|r\rangle\langle e| + \mathrm{H.c.} - \delta|r\rangle\langle r| + \chi\delta|e\rangle\langle e|$$
$$\mathcal{H}_t = \frac{\Omega_\mathrm{r}(t)}{2}|1\rangle\langle r| + \frac{\Omega_\mathrm{r}'(t)}{2}|0\rangle\langle r| + \frac{\Omega_\mathrm{d}\left(\mathrm{e}^{\mathrm{i}\Delta_\mathrm{d}t} + \mathrm{e}^{-\mathrm{i}\Delta_\mathrm{d}t}\right)}{2}|r\rangle\langle e| + \mathrm{H.c.} - \delta|r\rangle\langle r| + \chi\delta|e\rangle\langle e|$$

and I is the identity operator. Here, V denotes the strength of van der Waals interaction for Rydberg pair state $|rr\rangle$, and $\Omega_\mathrm{r}(t) = |\Omega_\mathrm{r}(t)|\mathrm{e}^{\mathrm{i}\phi(t)}$, $\Omega_\mathrm{r}'(t) = |\Omega_\mathrm{r}'(t)|\mathrm{e}^{\mathrm{i}\phi'(t)}$ are the laser Rabi frequencies. We stress a global drive of both laser fields, so as to eliminate the constraint of stepwise operations. Besides, two atoms are placed at short distances such that the interaction strength V is much larger than laser Rabi frequencies (i.e. $V \gg |\Omega_\mathrm{r}(t)|, |\Omega_\mathrm{r}'(t)|$), resulting in a strong suppression of simultaneous excitation of both atoms to the Rydberg state [38, 39]. In the following, we are interested in finding robust pulses $\Omega_\mathrm{r}(t), \Omega_\mathrm{r}'(t)$ that are insensitive to the variation of Doppler shift δ.

3. Doppler dephasing robust pulses

We proceed by addressing the suppression of Doppler error via the combination of gate protocols and optimal control methods [40–42]. A two-qubit CNOT gate can be realized by using numerically optimized continuous pulses $\Omega_\mathrm{r}, \Omega_\mathrm{r}', \Omega_\mathrm{d}$ with a series of tunable parameters. To implement a time-optimal gate that operates within a duration of T_g, if for the no-dressing case as discussed in our prior work [43], where the system follows the standard two-photon excitation model, states $|00\rangle$ and $|01\rangle$ would experience single-qubit rotations with two resonant couplings $\Omega_\mathrm{r}(t), \Omega_\mathrm{r}'(t)$, requiring $|00\rangle \to |00\rangle$ and $|01\rangle \to |01\rangle$ at $t = T_\mathrm{g}$. While states $|10\rangle$ and $|11\rangle$ are off-resonantly coupled due to the blockade constraint and global drive. We expect the exact conversion of $|10\rangle \to |11\rangle$ and $|11\rangle \to |10\rangle$ for a CNOT gate with optimal parameters. Finally, we can measure the fidelity of gate with a commonly-used definition as

$$F = \frac{1}{4}\mathrm{Tr}\left[\sqrt{\sqrt{\mathcal{O}}\rho\left(t = T_\mathrm{g}\right)\sqrt{\mathcal{O}}}\right] \tag{2}$$

having considered the average effect of four computational basis states $\{|00\rangle, |01\rangle, |10\rangle, |11\rangle\}$, where $\mathcal{O}$ is the ideal unitary matrix for the gate, and $\rho(t = T_\mathrm{g})$ is the realistic output density matrix at the end of the gate operation. To solve the dynamics of each basis state, we use the Liouville-von Neumann equation with Lindblad relaxation terms [44]

$$\partial\rho(t)/\partial t = -\mathrm{i}[\mathcal{H}, \rho] + \mathcal{L}_r[\rho] + \mathcal{L}_e[\rho] \tag{3}$$

Table 1. Optimized gate parameters for three laser amplitudes $\Omega_r(t), \Omega_r'(t), \Omega_d$ (in unit of $2\pi\times$MHz), laser phases $\phi(t), \phi'(t)$ (in unit of 2π) as well as the gate duration T_g (in unit of μs). In all cases, the dressing-field detuning is $\Delta_d \approx \Omega_d/0.698$ ensured by the insensitive condition. The blockade strength is $V/2\pi = 200$ MHz throughout. The last column presents the ideal gate fidelity in the absence of any decay ($\gamma_r = \gamma_e = 0$).

			$\Omega_r(t)$		$\Omega_r'(t)$		$\phi(t), \phi'(t)$				
Case	Type	T_g	Ω_{max}	ω	Ω'_{max}	ω'	δ_0	δ_1	δ_2	Ω_d	F(ideal)
no-dressing	linear	1.00	9.87	0.1946	10.0	0.1938	4.90	$\times$	$\times$	$\times$	0.999 45
	composite	0.62	9.19	0.1018	8.96	0.1026	−0.117	0.589	−0.0006	$\times$	0.999 59
with-dressing	linear	3.18	9.56	0.1007	9.59	0.1007	−4.97	$\times$	$\times$	195.7	0.997 26
	composite	3.60	9.89	0.1091	9.95	0.1093	−4.77	−0.57	−2.07	201.4	0.999 71

where

$$\mathcal{L}_r[\rho] = \sum_{i\in\{0,1,e\}} \left(L_{ir}\rho L_{ir}^\dagger - \frac{1}{2}\left[L_{ir}^\dagger L_{ir}\rho + \rho L_{ir}^\dagger L_{ir}\right]\right)$$
$$\mathcal{L}_e[\rho] = \sum_{j\in\{0,1\}} \left(L_{je}\rho L_{je}^\dagger - \frac{1}{2}\left[L_{je}^\dagger L_{je}\rho + \rho L_{je}^\dagger L_{je}\right]\right)$$

and $L_{ir} = \sqrt{\gamma_r/3}|i\rangle\langle r|$, $L_{je} = \sqrt{\gamma_e/2}|j\rangle\langle e|$ stands for Lindblad operators that correspond to the spontaneous emission from each excited state to each ground state.

In the presence of an auxiliary state $|e\rangle$ (with-dressing case), the optimization of pulses for the gate requires more tunable parameters, which makes the entire evolution difficult to satisfy. In this work, in order to ease the experimental implementation, we use smooth modulation for both laser amplitude $|\Omega_r^{(\prime)}(t)|$ and phase $\phi^{(\prime)}(t)$, and set the dressing field Ω_d as a constant value to be optimized. Specifically, we perform a smooth phase modulation whose slope also represents the two-photon detuning value [9, 45]. Two kinds of robust pulses are considered: one with a phase profile given by a linear function

$$\phi(t) = \delta_0 t \tag{4}$$

corresponding to a fixed two-photon detuning δ_0 to $|r\rangle$, and a second one with a composite phase profile

$$\phi(t) = \delta_0 t + \delta_1 \sin\left(\frac{4\pi t}{T_g}\right) + \delta_2 \cos\left(\frac{2\pi t}{T_g}\right) \tag{5}$$

which results in a more sufficient modulation for the two-photon detuning. We assume $\phi' = \phi$ for simplicity. Except for the varying phase, the varying amplitude depends on an assumption of smooth Gaussian profiles

$$|\Omega_r(t)| = \Omega_{max} e^{-\frac{(t-T_g/2)^2}{2\omega^2}}, |\Omega_r'(t)| = \Omega'_{max} e^{-\frac{(t-T_g/2)^2}{2\omega'^2}} \tag{6}$$

with $\Omega_{max}, \Omega'_{max}$ the maximal amplitudes and ω, ω' the pulse widths. Following [46], we choose the numerical genetic algorithm with single target of maximizing the gate fidelity F by globally optimizing all pulse parameters. Note that the intrinsic decay error due to finite lifetime of energy levels is also considered by numerical optimization, ensuring a minimal time-spent on intermediate excited states $|r\rangle$ and $|e\rangle$ [8]. In addition, we add the gate duration T_g as another quantity to be optimized which is surely limited by the maximal amplitudes. For constituting a practical gate that can reduce the spontaneous decay from excited states, we choose a slightly higher limitation for the two-photon Rabi frequency $(\Omega_{max}, \Omega'_{max})/2\pi \leqslant 10$ MHz, which enables the gate duration $T_g \leqslant 1.0\,\mu$s in the *no-e* cases [47]. While this duration scale will be prolonged in the *with-e* case due to the extra population exchange between $|r\rangle$ and $|e\rangle$ states.

The optimized gate parameters in no-dressing and with-dressing cases are presented in table 1, in which two different phase profiles (linear and composite) are applied. The amplitude and phase profiles are plotted in figures 2(b1)–(b4) and the corresponding infidelities $1 - F(\delta)$ as a function of δ are shown in figure 2(a). It is explicit that the standard two-photon scheme, i.e. *no-e* case has no robustness to the Doppler dephasing error, no matter how to modulate the laser phase profile. Thus, once $|\delta|$ grows, the infidelity reveals an exponential increase (also see figure 2 of [14]), quickly reaching as high as $\sim$0.1 at $|\delta|/2\pi = 1.0$ MHz. To quantify the performance of the dressing cases, figure 2(a) also presents the infidelity under the help of dressing fields by performing the same optimization of all gate parameters. Excitingly, we find that the ideal infidelity in both dressing cases remains a constant for any δ, strongly confirming the achievement of a perfect protection for the Doppler dephasing error. It is more interesting that, by implementing a sufficiently

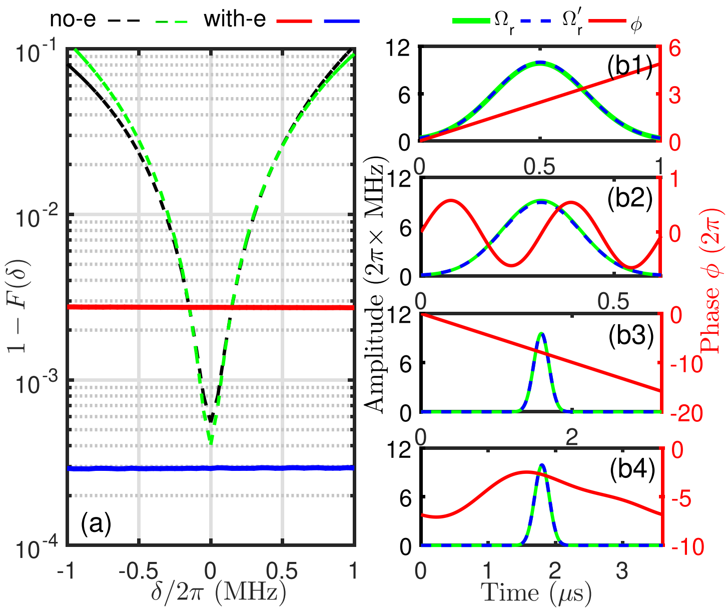

Figure 2. (a) Dependence of the gate infidelity $1 - F(\delta)$ on the Doppler shift δ in the absence of decay. Two no-dressing cases with linear (or composite) phase modulation are denoted by the black-dashed (or green-dashed) lines, marked by *no-e*. Similarly, for two *with-e* cases, results are denoted by red and blue solid lines. (b1–b4) Laser amplitudes and phase profiles with respect to the four cases in (a).

composite modulation (blue-solid) of the pulse phase, the infidelity can even outperform the linear modulation (red-solid) by one order of magnitude, staying at a very low level $\sim 3.0\times 10^{-4}$.

For completeness, we also calculate the time-integrated intermediate-state population. The total time-spent in Rydberg state $|r\rangle$ of the *no-e* case is quite large $P_r \approx (0.8372, 0.6536)\,\mu$s corresponding to the linear and composite profiles, which is mainly caused by a wide laser-amplitude modulation over the entire gate execution (see figures 2(b1) and (b2)). However, for the *with-e* protection mechanism with dressing fields, the real pulse widths ω, ω' are strongly narrowed although at the cost of a prolonged gate time (see figures 2(b3) and (b4)), which can achieve a much shorter time-spent in Rydberg states $P_r \approx (0.1133, 0.0742)\,\mu$s and auxiliary states $P_e \approx (0.0705, 0.0466)\,\mu$s as compared to two *no-e* cases. We point out that, although the average time-spent in the auxiliary state $|e\rangle$ has been deeply minimized by optimization during the dressing case, our gate may still suffer from a big decay error. Because the low-lying excited state $|e\rangle$ ($|5P_{1/2}\rangle$) is short-lived with a decay rate γ_e, typically 3 orders of magnitudes larger than γ_r of state $|r\rangle$, which ultimately limits the realistic gate fidelity. The discussion for this dominant decay error will be presented in section 5.2, and a prospective protocol with zero decay error is presented in section 6.

4. Application to more dressing cases

Doppler dephasing induced by the residual thermal motion of atoms occurs across various atomic systems, which dominantly limits the gate performance in the field of quantum computing [48, 49]. In section 3, we have used the atomic parameters corresponding to a ^{87}Rb atom with $|e'\rangle = |5P_{3/2}\rangle$ and $|e\rangle = |5P_{1/2}\rangle$, arising the sensitivity factor $\chi = 1.627$ ($\Omega_d/\Delta_d \approx 0.698$). In order to verify the generality of our scheme adapted for more atomic systems, we illustrate other double-dressing examples in Rb and Cs atoms (see table 2). Note that the sensitivity factor χ is crucial that determines the degree of off-resonant dressing between $|r\rangle$ and $|e\rangle$, consequently affecting the time-spent in these states. To analyze the role of χ, we newly optimize all gate parameters for cases (a) and (g) of table 2 as compared to the original case (c). As shown in figure 3, we find that cases (a) and (g) remain absolutely stable insensitivity to the variation of the Doppler shift δ, strongly confirming the existence of an efficient protection mechanism from state $|e\rangle$. However, once the insensitive condition is broken, the Doppler shift on $|r\rangle$ will no longer be perfectly protected, resulting in an exponential enhancement of the gate infidelity (see figure 3, dashed lines). In table 3, we give the three sets of optimized parameters in Rb and Cs atoms. For comparison, we further introduce another set of virtually optimized parameters with a large $\chi = 15$, which results in a far off-resonant coupling, i.e. $\Delta_d \gg \Omega_d$, ensuring a much shorter time-spent in $|e\rangle$. Numerical results based on the virtual case are displayed in figure 3 with full circles. It is obvious that this case is also perfectly robust to the Doppler dephasing error, and meanwhile benefits

Table 2. Choice of different intermediate states $|e'\rangle$ and auxiliary states $|e\rangle$ for two-qubit CNOT gates in ^{87}Rb and ^{133}Cs atoms. The effective two-photon wavevector is $\vec{k}_r = 2\pi(\lambda_{\mathrm{up}}^{-1} - \lambda_{\mathrm{lower}}^{-1})$, in which $\lambda_{\mathrm{up}}(\mathrm{nm})$ and $\lambda_{\mathrm{lower}}(\mathrm{nm})$ represent the laser wavelengths of upper and lower transitions respectively, and $\vec{k}_a = -2\pi/\lambda_a$, where $\lambda_a(\mathrm{nm})$ is the wavelength of the optical dressing fields. $\tau_e(\mu s)$ denotes the lifetime of the state $|e\rangle$. $\vec{k}_r$ and $\vec{k}_a$ are shown with a unit of $\mu\mathrm{m}^{-1}$. We highlight the selected three cases in bold in which case (c) has been studied in section 3.

	^{87}Rb				^{133}Cs			
Case	(a,b)		(c,d)		(e,f)		(g,h)	
$\|e'\rangle$	$5P_{1/2}$		$5P_{3/2}$		$6P_{1/2}$		$6P_{3/2}$	
λ_{up}	475		480		495		509	
λ_{lower}	795		780		895		852	
$\vec{k}_r$	5.324		5.035		5.673		4.969	
$\|e\rangle$	$5P_{1/2}$	$5P_{3/2}$	$5P_{1/2}$	$5P_{3/2}$	$6P_{1/2}$	$6P_{3/2}$	$6P_{1/2}$	$6P_{3/2}$
λ_a	475	480	475	480	495	509	495	509
$\|\vec{k}_a\|$	13.228	13.089	13.228	13.089	12.693	12.344	12.693	12.344
τ_e	0.158	0.150	0.158	0.150	0.200	0.174	0.200	0.174
χ	**1.484**	1.458	**1.627**	1.6	1.238	1.176	**1.554**	1.484

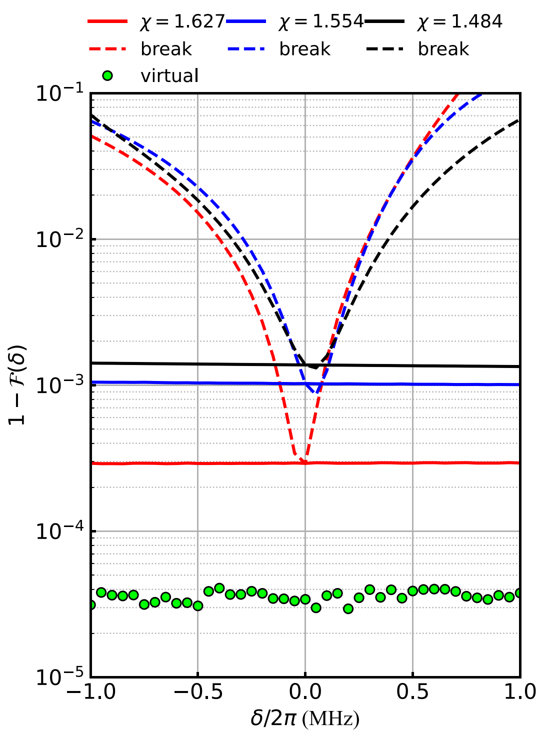

Figure 3. The gate infidelity $1 - F(\delta)$ for different sensitivity factors $\chi = (1.627, 1.484, 1.554)$ denoted by solid lines. The corresponding dashed lines present the breakdown of the insensitive condition by increasing χ to 15, while all optimized parameters are kept unvaried. In addition, a virtually optimized case with a large $\chi = 15$ is shown by full circles. No decay is included in the calculation.

from a lower infidelity $1 - F \sim 3 \times 10^{-5}$ due to the deep minimization of time-spent in state $|e\rangle$ at off-resonant condition.

Finally, we emphasize that the extension of this Doppler error erased protocol to more atomic sources (Rb, Cs) is possible, as long as a suitably dressing state $|e\rangle$ featuring an opposite but enhanced velocity sensitivity for the $|r\rangle \to |e\rangle$ transition can be found. Furthermore, we note that the ideal gate fidelity can even be improved to be > 0.9999 (the last column in table 3) if the insensitivity factor χ grows. This is interesting in the limit where a long-lived auxiliary state is dressed, such that the intrinsic decay error can be entirely avoided. In order to diminish the dissipative effect from the auxiliary state, in section 6., we introduce an improved protocol by dressing Rydberg state to a hyperfine ground state $|g\rangle$ (not a lower excited state) through the one-photon transition. The central idea of protocol is to avoid the large spontaneous decay from $|5P_{1/2}\rangle$ by replacing it with a more stable state.

Table 3. Optimized gate parameters based on the choice of different sensitivity factors $\chi = (1.627, 1.484, 1.554)$ in Rb and Cs atoms, corresponding to the dressing levels in Cases (c), (a) and (g) of table 2. Besides the optimized parameters, the required dressing-field detuning Δ_d, the average time-spent in Rydberg state denoted by $P_r(\mu s)$ and in auxiliary state denoted by $P_e(\mu s)$, the ideal gate fidelity F are also given in the last four columns. We highlight the last row in green suggesting an ideally large sensitivity factor $\chi = 15$ regardless of the realistic atomic energy levels. This choice can provide a pronounced improvement in the gate fidelity because of the far off-resonant coupling ($\Delta_d \gg \Omega_d$) to the auxiliary state $|e\rangle$.

Atom	χ	T_g	$\Omega_r(t)$		$\Omega'_r(t)$		$\phi(t), \phi'(t)$			Ω_d	Δ_d	P_r	P_e	F(ideal)
			Ω_{max}	ω	Ω'_{max}	ω'	δ_0	δ_1	δ_2					
Rb	1.627	3.60	9.89	0.1091	9.95	0.1093	−4.77	−0.57	−2.07	201.4	288.5	0.0742	0.0466	0.999 71
	1.484	3.59	9.70	0.1086	9.70	0.1080	−15.0	2.72	0.874	262.4	362.0	0.0896	0.0612	0.998 80
Cs	1.554	3.55	9.43	0.1073	9.47	0.1075	−7.37	0.54	−0.98	218.6	307.3	0.0977	0.0638	0.998 97
Virtual	15	2.12	10.00	0.2383	9.12	0.2573	10.00	−1.09	−0.15	240.0	945.4	0.2837	0.0192	0.999 97

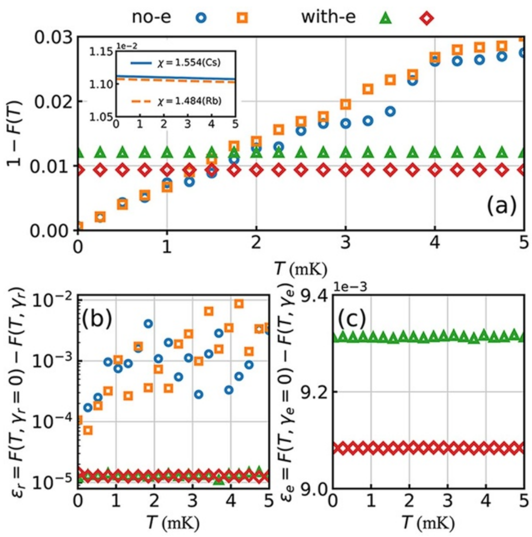

Figure 4. (a) The gate infidelity $1 - F(T)$ at different values of atomic temperature where the decays of Rydberg and dressing states are both included, corresponding to the four cases described in table 1. The inset of (a) shows infidelities at the cases of $\chi = 1.484$ and $\chi = 1.554$ (see table 3). (b), (c) Simulation of the realistic decay errors ε_r (for Rydberg state $|r\rangle$ at $\gamma_e = 0$) and ε_e (for auxiliary state $|e\rangle$ at $\gamma_r = 0$) under different T. For a given T, each point denotes an average over 300 random realizations. Here the specific decay rates considered are $\gamma_r = 1/\tau_r \approx 2.6$ kHz, $\gamma_e = 1/\tau_e \approx 2\pi \times 1.0$ MHz.

5. Realistic gate performance with robust pulses

5.1. Gate performance

To gain insight on how the Doppler dephasing error affects the realistic gate performance with robust pulses, we now include the spontaneous decays of Rydberg and dressing states at a finite temperature T. During the gate execution, both the ground-Rydberg and the ground-dressing transitions will inevitably suffer from atomic motional dephasing, which makes the real laser frequency perceived by the moving qubit atoms deviate from its ideal value [50]. This can be estimated as the level detuning changes δ and $\chi\delta$, respectively for Rydberg and auxiliary states. Although the actual Doppler shifts of two atoms are different due to the uncorrelated atomic velocities, our gate protocol suggests an independent protection for each Rydberg state with an individual dressing state, so the anti-symmetric detuning error does not work here [14]. The velocity $\vec{v}$ originates from finite temperature T of trapped atoms constituting an intrinsic source of randomness. Here we assume $\vec{v}$ is randomly drawn from a one-dimensional Gaussian distribution with width $v_{rms} = \sqrt{k_B T/m}$, where k_B is the Boltzmann constant and m is the mass of atoms. This choice arises the detuning changes $\delta = \vec{k}_r \cdot \vec{v}$ and $\chi\delta = (\vec{k}_r + \vec{k}_a) \cdot \vec{v}$. Both of them are also random values. Then we calculate the gate infidelity caused by residual thermal motion of atoms, represented by the relationship between $1 - F(T)$ and the atomic temperature T.

Numerical results are summarized in figure 4(a). We first focus on two *no-e* cases. As expected, the gate infidelity dramatically increases as T grows no matter how to modulate the phase profile [51]. Because without the use of protection mechanism, the gate protocol is ideally optimized in the absence of the Doppler error, i.e. at $T = 0$. As T increases, both the Rydberg decay error ε_r and the Doppler dephasing error are dominant. At $T = 5$ mK, we observe that these two errors contribute at the same level $\sim 10^{-2}$ (also see figure 4(b)), leading to the total infidelity as high as $1 - F \approx 0.03$. In contrast, for the newly-proposed *with-e* cases the infidelity perfectly preserves a constant for *any* temperature, which means the Doppler dephasing error has been truly erased that no longer depends on the temperature. Besides, we also note that, the selected choices ($\chi = 1.627, 1.484, 1.554$, see inset of figure 4(a)) for Rb and Cs atoms can all contribute a Doppler-error erased gate with the increasing of atomic temperatures.

Note that, the results over a very wide temperature range is schematically given in figure 4(a), only for presenting the absolute insensitivity of gate infidelity against the Doppler dephasing error for *any* temperature. Unfortunately, we observe the *with-e* protocols reveal better gate performance merely if $T > 1.5$ mK, which inherently makes the scheme worthless for current experiments that usually work in a cold environment. In the following, via a deep study of the major limitation as well as other error sources, we further propose a more relevant *with-g* protocol (by dressing with an auxiliary ground state) for achieving high-fidelity quantum gates, which also has significantly reduced insensitivity to the Doppler errors (see details in section 6).

5.2. Major obstacle

Despite the perfect insensitivity to the Doppler dephasing error, we should admit that there is a major obstacle in the gate protocol, originating from the choice of a short-lived dressing state $|e\rangle$ [52, 53]. For the chosen excited state $|e\rangle = |5P_{1/2}\rangle$ typically $\gamma_e \gg \gamma_r$, this will cause a larger decay error ε_e from the dressing state $|e\rangle$.

To address this issue, we separately characterize the gate infidelity by individually calculating two decay errors ε_r and ε_e, as a function of T in figures 4(b) and (c). By increasing the temperature, for no-dressing cases, the only Rydberg decay error quickly reaches as high as $\varepsilon_r \sim 10^{-2}$ at $T = 5$ mK, which means the random fluctuation δ from the atomic motional dephasing will significantly affect the time-spent in the Rydberg state, because no protection is performed for this state. However, with the help of dressing state $|e\rangle$, we observe that the ε_r (here $\gamma_e = 0$) obtains a big reduction and perfectly stays at $\sim 1.3 \times 10^{-5}$, outperforming the ε_r of two no-dressing cases by orders of magnitude due to the minimization of time-spent in the Rydberg state. In addition, the ε_r does not vary with T because $|r\rangle$ is fully protected in this case. Finally, we estimate the intermediate decay error ε_e from the dressing state $|e\rangle$ in figure 4(c) only for two *with-e* cases. To avoid additional errors from the Rydberg state, we set $\gamma_r = 0$. By varying T it is clear that the decay error ε_e can also remain a constant owing to the perfect protection; whilst, unfortunately it keeps at a quite high value $\sim 10^{-2}$, serving as the leading-order error source to the gate infidelity. This is actually a result of the short lifetime of $|e\rangle$ and can be completely avoided by replacing with a long-lived dressing state (see section 6). The complete robustness of ε_r and ε_e to *any* T values also indicates that the average time-spent in both states ($|r\rangle, |e\rangle$) can be preserved unvaried with the increase of T. Hence, our protocol is verified to be perfectly immune to the Doppler-dephasing error caused by atomic thermal motion.

Accounting for the major obstacle by ε_e in the dressing protocols, we have shown that, our protocol with dressing-field protection mechanism (dressing a lower excited state) would suffer from a relatively low gate fidelity $F(T) \sim 0.9906$ (see figure 4(a)) as compared to the no-dressing case for $T \leqslant 1.5$ mK; although its full robustness against the Doppler dephasing errors for *any* temperature is very remarkable. In order to achieve a higher gate fidelity along with strong robustness, we develop a promising proposal by dressing with a long-lived ground state, as presented in section 6.

5.3. Other detuning error sources

It is worth pointing out that during the gate execution, other error sources such as the ac Stark shift [55–57], the fluctuation in laser frequencies [58–60] and so on, also serve as an unknown detuning error that leads to the realistic two-photon detuning, which includes not only the Doppler shift term $\delta = -\vec{k}_r \cdot \vec{v}$, but also other unknown detunings δ'. For a typical two-photon transition system with a large intermediate detuning, a significant ac Stark shift occurs as a consequence of the uncompensated laser amplitude fluctuations [25]. According to our recent work [61], for a modest estimation of laser amplitude deviation $\sim 5.0\%$, this unknown detuning is about $2\pi \times 0.32$ MHz. To quantify the robustness of *with-e* gate performance against other detuning errors, figure 5(a) shows the ideal gate infidelity at $\delta = 0$ and $2\pi \times 1.0$ MHz by varying extra errors over a wide parameter range $\delta'/2\pi \in [-1.0, 1.0]$ MHz. The observed gate infidelity $1 - F(\delta')$ clearly varies with δ' due to the breakdown of the insensitive condition. Because the realistic detuning $\chi\delta$ of the dressing state $|e\rangle$ is irrelevant to δ' (just relevant to δ), making the robust gate no longer immune to these error sources. By increasing the values of $|\delta'|$, we find that the ideal gate infidelity has the same trend of exponential enhancement for different $\delta/2\pi = (0, 1.0)$ MHz. In general, this detuning error source contributes at the level of $< 10^{-3}$, which is much smaller than the decay error ε_e by more than one order of magnitude, and is therefore not very important. This can be verified further by including the effect of

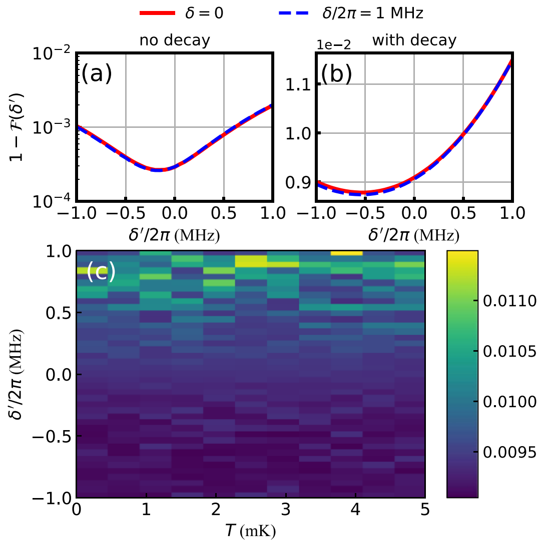

Figure 5. (a), (b) The infidelity of Doppler-error erased gates $1-F(\delta')$ as a function of other detuning fluctuation δ', where the Doppler shift is $\delta=0$ and $\delta/2\pi=1.0$ MHz, for the ideal case without decay and for the realistic case with spontaneous decays, respectively. (c) The realistic gate infidelity $1-F$ as a function of both T and δ'. Every point (T_j,δ_j') in the color plot is obtained by using an average over 300 random samplings, individually extracted from the range of a one-dimensional Gaussian distribution with $v_{\rm rms}=\sqrt{k_{\rm B}T_j/m}$ for T_j and a uniform distribution of $[-\delta_j',+\delta_j']$ for δ_j'.

spontaneous decays. In figure 5(b), we show the realistic infidelity over a range of detuning fluctuations δ'. As expected, the total gate infidelity maintains around $\sim 10^{-2}$, confirming the trivial impact from other detuning errors compared to the dominant decay error ε_e.

We also consider the realistic gate infidelity in the presence of both Doppler error (induced by a finite temperature T) and other detuning errors for completeness. Figure 5(c) presents the gate performance with composite phase modulation ($\chi=1.627$) in the *with-e* case. It is clear that the infidelity numbers can always maintain around 0.01 in the presence of significant detuning imperfections or Doppler dephasing errors, which indicates a powerful robustness of our gate protocol to any magnitude of errors on the two-photon detuning.

As compared with the traditional three-photon Doppler-free scheme [26], we may expect the overall Doppler shift is automatically zero based on the starlike geometry, i.e. $\delta=0$. However, the uncompensated Doppler shifts in one- or three-photon detunings would induce extra ac Stark shift error δ' that allows the three-photon scheme to be not absolutely robust to the change of atomic temperature. A rough estimation shows that, even for $T=1$ K with a maximal δ' adding to the Rydberg state of about 0.1 MHz, the infidelity $F(\delta'=0)-F(\delta')$ is only $\sim 3.5\times 10^{-5}$ in the *no-e* case using the optimized composite pulses, confirming the feasibility of three-photon Doppler-free scheme although it is technically more demanding and therefore impractical.

6. Dressing with long-lived ground states

In section 5, we have shown the error-erasing strategy of Doppler dephasing error in Rydberg quantum gates. However, the major weakness of which lies in a large decay error $\varepsilon_e\sim 0.01$ from the intermediate dressing state $|e\rangle$, resulting in the ultimate gate fidelity $F\approx 0.9906$ even at low temperatures. In order to overcome this decay error and improve the gate fidelity to a better level, we develop a modified protocol by replacing the auxiliary state to be a stable ground state, so as to essentially avoid this dominant error. In figure 6(a), we assume that the qubits are encoded into two hyperfine atomic ground states $|0\rangle$ and $|1\rangle$, and the traditional excitation to Rydberg $|s\rangle$ states is driven by a two-photon process. When two atoms are prepared in the pair state $|ss\rangle$, they will experience a natural two-body Förster resonance by obeying $|ss\rangle \rightleftarrows |pp'\rangle$ with a dipole–dipole interaction strength V [62–64]. Here, due to the transition selection rule, we remark that two dressing fields $\Omega_{\rm d}$ should drive the coupling between $|p\rangle,|p'\rangle$ and $|g\rangle$ via a 297 nm ultraviolet laser [65] since state $|s\rangle$ is transition-forbidden. This new choice provides $\vec{k}_a=-2\pi/\lambda_{297}=21.156\mu m^{-1}$ ($\vec{k}_r$ is the same), arising a larger sensitivity factor $\chi=3.202$ when $\Omega_{\rm d}/\Delta_{\rm d}\approx 0.463$.

Now, the total Hamiltonian for the improved gate protocol, reads

$$\mathcal{H}=\mathcal{H}_c\otimes I+I\otimes\mathcal{H}_t+V(|ss\rangle\langle pp'|+|pp'\rangle\langle ss|) \tag{7}$$

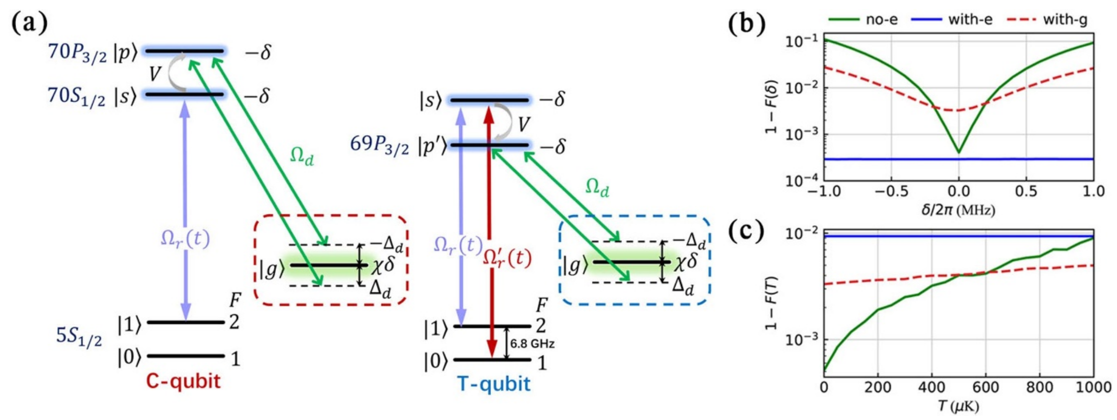

Figure 6. (a) The gate protocol that dresses a long-lived ground state $|g\rangle = |5S_{1/2}, F = 2, m_F = -1\rangle$ instead of a short-lived excited state $|e\rangle$. The qubit states $|0\rangle$ and $|1\rangle$ are same (see figure 1). A dipole–dipole interaction V drives the exchange coupling between two Rydberg pair states $|ss\rangle \rightleftarrows |pp'\rangle$ (e.g. $|70S_{1/2}70S_{1/2}\rangle \rightleftarrows |70P_{3/2}69P_{3/2}\rangle$) [54]. Here states $|p\rangle$ and $|p'\rangle$ (noticeably $|s\rangle$ is not protected) are directly protected via a one-photon dressing with the ground state $|g\rangle$. The Rydberg decay rates from $|s\rangle$ and $|p, p'\rangle$ are $\gamma_s = 2.6$ kHz, $\gamma_{p,p'} = 1.3$ kHz, and the dipole–dipole interaction strength is $V = 2\pi \times 200$ MHz. (b)–(c) Gate performance based on the ground-dressing protocol are given by the red-dashed line, denoted as *with-g*. For comparison, the original *no-e* and *with-e* protocols using the case of composite phase modulation, are also presented. (b) The infidelity $1 - F(\delta)$ as a function of the Doppler shift δ in the absence of Rydberg decay. (c) The realistic gate infidelity $1 - F(T)$ as a function of T, including the spontaneous decays from all Rydberg levels.

where single-qubit Hamiltonians are

$$
\begin{aligned}
\mathcal{H}_c &= \frac{\Omega_{\mathrm{r}}(t)}{2}|1\rangle\langle s| + \frac{\Omega_{\mathrm{d}}\left(\mathrm{e}^{\mathrm{i}\Delta_{\mathrm{d}}t} + \mathrm{e}^{-\mathrm{i}\Delta_{\mathrm{d}}t}\right)}{2}|p\rangle\langle g| + \mathrm{H.c.} \\
&\quad - \delta\left(|s\rangle\langle s| + |p\rangle\langle p|\right) + \chi\delta|g\rangle\langle g| \\
\mathcal{H}_t &= \frac{\Omega_{\mathrm{r}}(t)}{2}|1\rangle\langle s| + \frac{\Omega_{\mathrm{r}}'(t)}{2}|0\rangle\langle s| + \frac{\Omega_{\mathrm{d}}\left(\mathrm{e}^{\mathrm{i}\Delta_{\mathrm{d}}t} + \mathrm{e}^{-\mathrm{i}\Delta_{\mathrm{d}}t}\right)}{2}|p'\rangle\langle g| + \mathrm{H.c.} \\
&\quad - \delta\left(|s\rangle\langle s| + |p\rangle\langle p|\right) + \chi\delta|g\rangle\langle g|,
\end{aligned}
$$

respectively. Similarly, numerical simulation adopts the Liouville-von Neumann equation: $\partial\rho(t)/\partial t = -i[\mathcal{H},\rho] + \mathcal{L}_s[\rho] + \mathcal{L}_p[\rho]$ with two Lindblad relaxation terms

$$
\begin{aligned}
\mathcal{L}_s[\rho] &= \sum_{i\in\{0,1,g\}}\left(L_{is}\rho L_{is}^{\dagger} - \frac{1}{2}\left[L_{is}^{\dagger}L_{is}\rho + \rho L_{is}^{\dagger}L_{is}\right]\right) \\
\mathcal{L}_p[\rho] &= \sum_{i\in\{0,1,g\}}\sum_{j\in\{p,p'\}}\left(L_{ij}\rho L_{ij}^{\dagger} - \frac{1}{2}\left[L_{ij}^{\dagger}L_{ij}\rho + \rho L_{ij}^{\dagger}L_{ij}\right]\right)
\end{aligned}
$$

where the Lindblad operators are $L_{is} = \sqrt{\gamma_s/3}|i\rangle\langle s|$, $L_{ip} = \sqrt{\gamma_p/3}|i\rangle\langle p|$, $L_{ip'} = \sqrt{\gamma_{p'}/3}|i\rangle\langle p'|$, describing the Rydberg state decays. By extending to the new protocol that dresses with a hyperfine ground state $|g\rangle$, we apply numerical optimization to both laser amplitude and (composite) phase profiles, in which the parameters are (all units are the same as in table 1)

$$
\begin{aligned}
&\Omega_{\max} = 2\pi\times 8.39, \quad \omega = 0.1179 \\
&\Omega_{\max}' = 2\pi\times 7.94, \quad \omega' = 0.1287 \\
&\Omega_{\mathrm{d}} = 2\pi\times 163, \quad \Delta_{\mathrm{d}} = 2\pi\times 352 \\
&\delta_0 = -2\pi\times 14.81, \quad \delta_1 = 2\pi\times 1.16 \\
&\delta_2 = -2\pi\times 0.014, \quad T_{\mathrm{g}} = 0.8.
\end{aligned}
$$

We note that this new protocol benefits from a much shorter gate duration ($T_{\mathrm{g}} = 0.8\,\mu$s) for minimizing the time-spent in Rydberg states only, more similar as the no-dressing case.

To see whether this *with-g* protocol is fully robust to the Doppler dephasing error and meanwhile manifests as a high-fidelity gate, we first simulate the ideal infidelity $1 - F(\delta)$ as a function of δ in figure 6(b), marked by the red-dashed line. The best Doppler-error erased case (blue line) with $\chi = 1.627$ for Rb atoms is comparably displayed, which undoubtedly shows a complete robustness to the variation of Doppler shift δ.

However, we observe that this new *with-g* protocol reveals some robustness as compared to the *no-e* case against the change of δ values, unfortunately it is unable to be absolutely robust. This can be readily understood by the design of two dressing fields, which only drive the Rydberg $|p, p'\rangle$ states so as to achieve the protection from motional dephasing merely for these two states. While other Rydberg $|s\rangle$ states can feel the same magnitude of Doppler errors, which are not directly protected by the presence of $|g\rangle$. Thus, the resulting infidelity will no longer be fully immune to the Doppler dephasing error, revealing a small increase with the Doppler shift $|\delta|$.

Next we proceed by studying the realistic gate performance $1 - F(T)$ in the presence of both Doppler and Rydberg decay errors. Figure 6(c) shows the realistic gate infidelities by averaging over sufficient ($N = 300$) random samplings of atomic velocity for each T in the range of [0,1000] μK. The *no-e* and *with-e* protocols are the same as in figure 4(a). Clearly, at low temperatures $T < 1000\,\mu$K, the *with-e* protocol has no advantages to maintain a higher infidelity than the *no-e* case because of the dominant decay error ($\varepsilon_e \sim 0.01$) of state $|e\rangle$. However, we observe that the *with-g* protocol can explicitly provide a lower infidelity although at the cost of a small loss of robustness due to the unprotected state $|s\rangle$, outperforming the *with-e* case for any temperature. In addition, it is also better than *no-e* as long as $T > 500\,\mu$K. This is expected because the improved *with-g* protocol benefiting from a non-lossy ground-state dressing, can effectively avoid the large spontaneous decay from intermediate excited states, resulting in a more acceptable gate fidelity $F \approx 0.9965$ at $T = 50\,\mu$K. Even if the temperature is increased to 500 μK, the gate fidelity can be maintained at $F \approx 0.9960$, which implies the strong (not perfect) robustness of scheme to the change of Doppler shifts. By now, we have realized two-qubit CNOT gates featuring both high fidelity and strong insensitivity for a wide temperature range up to $\sim$1000 μK. This result can significantly decrease the temperature constraint for implementing quantum gates with cold atoms in the future.

7. Larger laser amplitudes

To further improve the practical relevance of scheme which can reveal advantages for a typical temperature $\sim$10 μK, in this section, we discuss the realistic gate performance by using higher two-photon laser amplitudes up to $(\Omega_{\max}, \Omega'_{\max})/2\pi \leqslant 20$ MHz, possibly done by ultrafast pulsed-laser technique [66–68], and show that both the *with-e* and *with-g* protocols can further be improved for colder temperatures owing to the substantial decrease of time-spent in the intermediate excited and Rydberg states.

To perform a deep optimization, here we additionally introduce a slightly more general ansatz for the phase profile, given by

$$\phi(t) = \delta_0 t + \delta_1 \sin\left(\frac{4\pi t}{T_g}\right) + \delta_2 \cos\left(\frac{\alpha\pi t}{T_g}\right) \tag{8}$$

where coefficient α is added for a fine tuning, and a smoothly-modulated Gaussian waveform for laser amplitudes is kept. Inspired by the results in the section 3, we note that the *with-e* (composite) protocol tends to require the laser pulse having a narrowed peak with a long tail for minimizing the intermediate-state population, e.g. for $\chi = 1.627$, the total time-spent in the Rydberg and auxiliary states is $(P_r, P_e) \approx (0.0884, 0.0554)\,\mu$s. In contrast, the *with-g* protocol is driven by using a relatively global pulse within a shorter gate time (more similar to the no-dressing case), which arises $(P_p, P_s) \approx (1.15 \times 10^{-4}, 0.1691)\,\mu$s when $\chi = 3.202$. We emphasize these time-spent values are obtained for the cases with spontaneous decays. Here, we re-optimize all gate parameters for two protocols with higher laser amplitudes, denoted as *with-e-improve* and *with-g-improve*, respectively.

In figures 7(a) and (b), the realistic gate infidelity $1 - F(T)$ as a function of T are separately given with the corresponding gate parameters summarized in table 4. With larger laser amplitudes, we clearly find a significantly improved gate quality, greatly outperforming the original *with-e* and *with-g* protocols. For example, in figure 7(a), the *with-e-improve* featuring complete robustness, has a higher fidelity of $F \approx 0.9955$ for *any* temperature, which reduces the infidelity number by 52.1% as compared to the *with-e* case. This improvement arises from the strong suppression of the time-spent $(P_r, P_e) \approx (0.0264, 0.0209)\,\mu$s on the intermediate lossy states, less than half of the time of the *with-e* case, which leads to a smaller decay error. Remarkably, results turn to be more exciting when the *with-g-improve* protocol is applied, see figure 7(b). The realistic gate infidelity preserves below 10^{-4} for any T within the range of $[0, 50]\,\mu$K, and even retains $F \approx 0.99991$ at $T = 50\,\mu$K. This development is mainly contributed by minimizing the time-spent on the unprotected Rydberg state $|s\rangle$ which serves as the dominant decay error for the gate implementation. We emphasize that, in this protocol there exists a strong time-spent minimization on the excited states leading to $(P_p, P_s) \approx (5.53 \times 10^{-4}, 0.1397)\,\mu$s. Here, the average time on state $|s\rangle$ has been significantly decreased by 17.4% (the impact of state $|p\rangle$ is negligible), so in contrast to *with-g*, the realistic gate infidelity can be reduced by several orders of magnitude. A strong robustness can also be seen for this case.

Table 4. Coefficients of the optimized laser pulses $\Omega_{\max}$, $\Omega'_{\max}$, Ω_d and $\phi(t),\phi'(t)$ and laser phases $\phi(t),\phi'(t)$ for the improved schemes (*with-e-improve* and *with-g-improve*) using larger laser amplitudes. The last column presents the realistic gate fidelity at $T=0$. Other parameters are given in table 1.

Case	Auxiliary state	T_g	$\Omega_r(t)$		$\Omega'_r(t)$		$\phi(t),\phi'(t)$						
			$\Omega_{\max}$	ω	$\Omega'_{\max}$	ω'	δ_0	δ_1	δ_2	α	Ω_d	Δ_d	F(realistic)
with-e-improve	excited state $\vert e\rangle$	2.54	19.64	0.0769	19.29	0.0768	−10.44	1.93	16.56	1.288	225.53	323.11	0.99 547
with-g-improve	ground state $\vert g\rangle$	1.14	19.85	0.1179	19.38	0.1202	20.0	0.90	−15.99	0.002	173.36	374.42	0.99 998

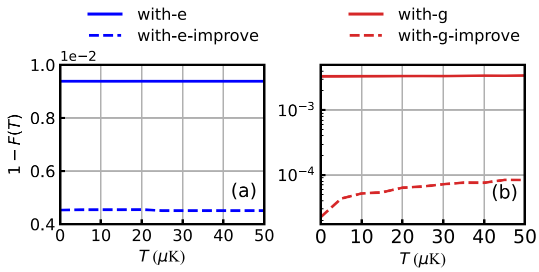

Figure 7. Gate performance with larger laser amplitudes. (a)–(b) The realistic gate infidelity $1-F(T)$ as a function of T, corresponding to the lower excited-state dressing and ground-state dressing cases, respectively. For comparison, the original cases (*with-e* and *with-g*) are represented by solid lines, while the improved *with-e-improve* and *with-g-improve* cases are indicated by dashed lines, whose parameters are given in table 4.

To shortly conclude, these improved protocols with larger laser amplitudes hold great promise for higher-quality Rydberg quantum gates. The completely robust *with-e-improve* protocol can fundamentally relax the temperature requirement for quantum gate operations. And the strong robustness in *with-g-improve* protocol is able to achieve a super-high gate fidelity for colder temperatures, possibly reaching a new milestone for two-qubit quantum gates in the neutral-atom computing platform. Both of them deserve the experimental demonstration in the near future.

8. Conclusion and outlook

So far, the ground-Rydberg dephasing error from finite atomic temperature is believed to be an ultimate limitation for the observed gate fidelity; however, it is rarely mitigated unless advanced technologies of atomic cooling and trapping are developed [69–71]. In this work, we use the protection scheme first proposed by Finkelstein and coworkers [29] to demonstrate a family of high-fidelity Doppler-error erased gates, enabled by cleverly dressing with an auxiliary state that protects the Rydberg state from Doppler dephasing errors. Based on the powerful optimal control strategy, we present several dressing protocols in alkaline Rb and Cs atoms that implement two-qubit CNOT gates using global modulations of both laser amplitude and phase profiles [72]. All protocols are fully robust to the Doppler dephasing errors yet at the cost of a slightly large decay error from the intermediate auxiliary state, which fundamentally restricts the attainable gate fidelity of $F\approx 0.9906$ for *any* temperature. To improve the practical relevance of protocols, we show that it is more interesting to replace with a non-lossy ground state (as the auxiliary state) to mitigate such incoherent spontaneous decay error achieving two-qubit CNOT gates with 0.9960 fidelity even at $T=500\,\mu$K, although the perfect insensitivity to Doppler errors would be slightly broken due to the existence of other unprotected Rydberg states. Finally, we note that robust pulses with a larger amplitude can enable significant improvements to the gate performance, suggesting a promise to the super-high gate fidelity of 0.99 991 for $T=50\,\mu$K.

This work can strongly relax the temperature constraint for achieving high-fidelity Rydberg gates by fully erasing the effect of Doppler dephasing error at *any* temperature, and would be worthwhile for future experimental demonstration. Before ending, we have to admit that our gate protocol will be passively impacted by other technical imperfections [73, 74]. For example, to completely quantify the gate performance under finite temperatures, we also study the error sources from the fluctuated interaction and the laser amplitude inhomogeneity. Both of them are induced by the thermal motion of atoms. Results in appendix B explicitly show that our new protocols do not have explicitly reduced insensitivity to these errors. However, a gate with complete robustness to certain error sources is enough useful, especially to the ground-Rydberg dephasing error which plays a dominant role for high-fidelity quantum information processing in scalable neutral-atom platforms [75, 76]. We believe such a protocol dealing with inhomogeneous Doppler dephasing could be utilized to explore other fault-tolerant mechanisms in many more platforms.

Data availability statement

All data that support the findings of this study are included within the article (and any supplementary files).

Acknowledgments

We acknowledge financial support from the Innovation Program for Quantum Science and Technology 2021ZD0303200; the NSFC under Grants No. 12234014, 12174106, 11474094, 11104076 and 11654005; the National Key Research and Development Program of China under Grant No. 2016YFA0302001; the Natural Science Foundation of Chongqing (No. CSTB2024NSCQ-MSX1117); the Shanghai Science and Technology Innovation Project (No. 24LZ1400600); the Science and Technology Commission of Shanghai Municipality under Grant No.18ZR1412800; the Shanghai Municipal Science and Technology Major Project under Grant No. 2019SHZDZX01 and the Shanghai talent program.

Appendix A. Derivation of the insensitive condition

Insensitive condition.—We start by deriving the insensitivity condition. To ease the derivation we assume that the Rydberg state $|r\rangle$ would experience an inhomogeneous energy shift $-\delta$ due to the inevitable Doppler shift induced by the residual thermal motion of qubit atoms, where $\delta = \vec{k}_r \cdot \vec{v}$ ($\vec{k}_r$ is the two-photon wavevector and $\vec{v}$ denotes atomic velocity). The addition of an auxiliary state $|a\rangle$ leads to a new subspace $\{|r\rangle, |a\rangle\}$ based on which we introduce a coherence protection mechanism, i.e. the double-dressing scheme as proposed and experimentally verified by Finkelstein *et al* [29]. Here we specifically discuss the double-dressing scheme that can be applied for constructing a high-quality Doppler-error erased gate. For an unknown shift $-\delta$ on $|r\rangle$, the auxiliary state $|a\rangle$ will obtain a similar shift $\delta' = (\vec{k}_r + \vec{k}_a) \cdot \vec{v}$ originating from the same source of inhomogeneity of atomic velocity. Since we require $\delta' = \chi\delta$ with $\chi = |1 + \vec{k}_a/\vec{k}_r|$ a dimensionless sensitivity factor, the dressing-field wavevector $\vec{k}_a$ should be opposite to $\vec{k}_r$ meanwhile requiring a larger amplitude $|\vec{k}_a| > |\vec{k}_r|$.

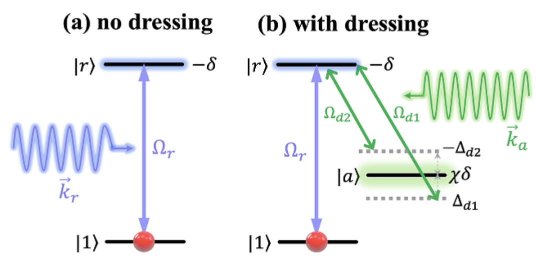

Figure 8. Coherence protection mechanism. (a) No dressing case: Single atom without dressing field is composed by the ground state $|1\rangle$ and the Rydberg state $|r\rangle$, which are coupled by a two-photon Rabi frequency Ω_r. The overall (two-photon) transition frequency shift is denoted by $-\delta$ due to the residual thermal motion of atoms at finite temperature. (b) With dressing case: Two dressing fields with Rabi frequencies Ω_{d1} and Ω_{d2} and opposite detunings Δ_{d1} and $-\Delta_{d2}$, are applied to protect state $|r\rangle$ from motional dephasing. The auxiliary state $|a\rangle$ experiences an opposite and possibly larger transition frequency shift $\chi\delta$, where $\chi = |1 + \vec{k}_a/\vec{k}_r|$ denotes a sensitivity factor.

The double-dressing scheme as shown in figure 8(b), involves a pair of dressing fields Ω_{d1} (detuned by Δ_{d1}) and Ω_{d2} (detuned by $-\Delta_{d2}$). The state $|r\rangle$ is coupled to $|a\rangle$ by the dressing fields, arising the total Hamiltonian in the subspace $\{|r\rangle, |a\rangle\}$ given by $\mathcal{H}_a = \mathcal{H}_0 + \mathcal{H}_1$, where

$$\mathcal{H}_0 = \begin{bmatrix} -\delta & 0 \\ 0 & \chi\delta \end{bmatrix} \tag{A1}$$

$$\mathcal{H}_1 = \left(\frac{\Omega_{d1}}{2} e^{i\Delta_{d1}t} + \frac{\Omega_{d2}}{2} e^{-i\Delta_{d2}t} \right) \begin{bmatrix} 0 & 1 \\ 1 & 0 \end{bmatrix}. \tag{A2}$$

To simplify the subsequent derivation, we rewrite $\mathcal{H}_0$ into a matrix form as

$$\mathcal{H}_0 = \frac{\delta}{2} \left([\chi - 1] \begin{bmatrix} 1 & 0 \\ 0 & 1 \end{bmatrix} - [\chi + 1] \begin{bmatrix} 1 & 0 \\ 0 & -1 \end{bmatrix} \right) \tag{A3}$$

and rotate the system around the y axis by using

$$U=\frac{1}{\sqrt{2}}\begin{bmatrix}1 & -1\\ 1 & 1\end{bmatrix} \tag{A4}$$

such that the rotated Hamiltonian transforming to the σ_x representation, takes form of

$$\begin{aligned}\mathcal{H}_a^R &= U^\dagger\mathcal{H}_aU=U^\dagger\left(\mathcal{H}_0+\mathcal{H}_1\right)U\\ &=\left[\frac{\Omega_{\mathrm{d1}}}{2}\left(\cos\Delta_{\mathrm{d1}}t+i\sin\Delta_{\mathrm{d1}}t\right)+\frac{\Omega_{\mathrm{d2}}}{2}\left(\cos\Delta_{\mathrm{d2}}t-i\sin\Delta_{\mathrm{d2}}t\right)\right]\\ &\quad\times S_z+\frac{\delta}{2}\left(\left[\chi-1\right]I+\left[\chi+1\right]S_x\right)\end{aligned} \tag{A5}$$

where I is the identity, and

$$S_x=\begin{bmatrix}0 & 1\\ 1 & 0\end{bmatrix}\ S_y=\begin{bmatrix}0 & -i\\ i & 0\end{bmatrix}\ S_z=\begin{bmatrix}1 & 0\\ 0 & -1\end{bmatrix}.$$

Next, after introducing a unitary transformation operator for $\mathcal{H}_1$ only,

$$\begin{aligned}U^{'}\left(t\right)&=\exp\left(-i\int_0^t U^\dagger\mathcal{H}_1\left(t_1\right)Udt_1\right)\\ &=\exp\left(-iS_z\left[\frac{\Omega_{\mathrm{d1}}}{2\Delta_{\mathrm{d1}}}\left(\sin\Delta_{\mathrm{d1}}t-i\cos\Delta_{\mathrm{d1}}t+i\right)+\frac{\Omega_{\mathrm{d2}}}{2\Delta_{\mathrm{d2}}}\left(\sin\Delta_{\mathrm{d2}}t+i\cos\Delta_{\mathrm{d2}}t-i\right)\right]\right)\end{aligned} \tag{A6}$$

we obtain the total Hamiltonian under the interaction picture

$$\begin{aligned}\mathcal{H}_a^I=\frac{\delta}{2}&\left[\left(\chi-1\right)I+\left(\chi+1\right)\left(S_+\mathrm{e}^{\left(\mathrm{i}z_1\sin\Delta_{\mathrm{d1}}t-\mathrm{i}z_1^{'}\cos\Delta_{\mathrm{d1}}t-z_1\right)}\right.\right.\\ &\left.\left.+S_+\mathrm{e}^{\left(\mathrm{i}z_2\sin\Delta_{\mathrm{d2}}t+\mathrm{i}z_2^{'}\cos\Delta_{\mathrm{d2}}t+z_2\right)}+H.c.\right)\right]\end{aligned} \tag{A7}$$

where $z_1=\Omega_{\mathrm{d1}}/\Delta_{\mathrm{d1}}$, $z_1^{'}=\mathrm{i}\Omega_{\mathrm{d1}}/\Delta_{\mathrm{d}}$, $z_2=\Omega_{\mathrm{d2}}/\Delta_{\mathrm{d2}}$, $z_2^{'}=\mathrm{i}\Omega_{\mathrm{d2}}/\Delta_{\mathrm{d2}}$, S_+ is the Pauli matrix.

Utilizing the Jacobi–Anger identity

$$\mathrm{e}^{\pm\mathrm{i}z\sin(\Delta_{\mathrm{d}}t)}=\sum_{n=-\infty}^{+\infty}J_n\left(z\right)\mathrm{e}^{\pm\mathrm{i}n\Delta_{\mathrm{d}}t} \tag{A8}$$

we reduce equation (A7) to the first-order in the Magnus expansion [77]

$$\begin{aligned}\mathcal{H}_a^{(1)}&=\frac{1}{T}\int_0^T\mathcal{H}_a^I\left(t_1\right)\mathrm{d}t_1\\ &=\frac{\delta}{2}\left[\left(\chi-1\right)I+J_0\left(z_1\right)J_0\left(z_1^{'}\right)\left(\chi+1\right)\left(S_+\mathrm{e}^{-z_1}+S_-\mathrm{e}^{z_1}\right)\right.\\ &\quad\left.+J_0\left(z_2\right)J_0\left(z_2^{'}\right)\left(\chi+1\right)\left(S_+\mathrm{e}^{z_2}+S_-\mathrm{e}^{-z_2}\right)\right].\end{aligned} \tag{A9}$$

To find the insensitive condition we require the eigenvalues of $\mathcal{H}_a^{(1)}$ vanish (i.e. independent of δ). By assuming two dressing fields with equal amplitudes and opposite detunings, i.e. $\Omega_{\mathrm{d}}=\Omega_{\mathrm{d1}}=\Omega_{\mathrm{d2}}$, $\Delta_{\mathrm{d}}=|\Delta_{\mathrm{d1}}|=|\Delta_{\mathrm{d2}}|$, the first-order reads

$$\mathcal{H}_a^{(1)}=\frac{\delta}{2}\left[\left(\chi-1\right)I+2J_0\left(z\right)\left(\chi+1\right)\left(S_+\mathrm{e}^{-z_1}+S_-\mathrm{e}^{z_1}\right)\right]$$

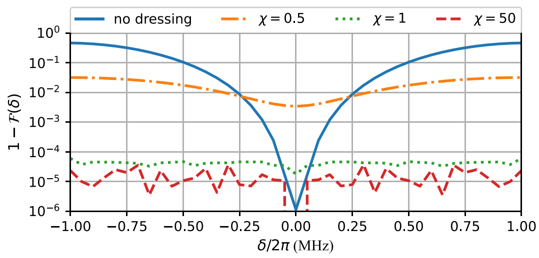

Figure 9. The infidelity $1-F(\delta)$ in the absence of any decay with different choices of $\chi=(0.5,1.0,50)$. The no dressing case is shown for comparison. All pulse parameters are found in table 5.

Table 5. Coefficients for plotting figure 9. The transfer duration τ is fixed to 1.0 μs.

		with dressing		
($2\pi\times$MHz)	no dressing	$\chi=0.5$	$\chi=1$	$\chi=50$
Ω_r	1	10	3	4
Ω_d	/	200	85	183
Δ_d	/	45	35	460

in which the general insensitive condition occurs at

$$J_0(z_1)=\frac{(\chi-1)}{2(\chi+1)}. \tag{A10}$$

Numerical verification.—To verify the validity of the insensitive condition (A10), we apply it for achieving the population transfer in a single atom, in order to see whether the transfer process is perfectly robust to the variation of energy shift δ. Consider a single atomic qubit comprising $|1\rangle$ and $|r\rangle$, as displayed in figure 8(a). The atom initially in $|1\rangle$, would experience a typical state rotation $|1\rangle\to|r\rangle\to|1\rangle$ after adopting a $2n\pi$ pulse ($\Omega_\mathrm{r}\tau=2n\pi$, τ is the transfer duration, n is a tunable integer). However, since the atoms are not stationary, their inhomogeneous velocity distribution leads to Doppler dephasing which reduces the fidelity of the population transfer. In figure 9 we numerically calculate the infidelity of state transfer by following the master equation $\mathrm{d}\rho/\mathrm{d}t=-i[\mathcal{H}_a,\rho]$ in the absence of any decay ($\gamma=0$), as a function of the Doppler shift δ. Depending on the definition of $\chi=|1+\vec{k}_a/\vec{k}_r|$, without loss of generality, we adopt the sensitivity factor $\chi=(0.5,1.0,50)$ as examples. Note that in the absence of dressing fields the transfer infidelity $1-F$ has an exponential enhancement with $|\delta|$ and is quickly close to 0.5 when the frequency shift $|\delta|/2\pi$ increases to 1.0 MHz. However, with the help of double-dressing protection scheme the insensitivity of the infidelity could be dramatically improved which implies that the insensitive condition can indeed make the system insensitive to the Doppler dephasing, achieving a perfect protection from the Doppler dephasing error.

Moreover, we find that the exact ratio between Ω_d and Δ_d caused by a different sensitivity factor χ, is quite different. For a small $\chi=0.5$ we have $\Omega_\mathrm{d}/\Delta_\mathrm{d}\approx 4.443$ and therefore the dressing state becomes near resonance there. The addition of double-dressing fields will severely affect the original state rotation between $|1\rangle$ and $|r\rangle$, arising a poor infidelity number $\sim 10^{-2}$. While for $\chi=1$, according to equation (A10), we have $\Omega_\mathrm{d}/\Delta_\mathrm{d}\approx 2.405$. The resulting infidelity as shown in figure 9, stays independent of δ and achieves a very low number $<10^{-4}$. For a larger $\chi=50$ which leads to $\Omega_\mathrm{d}/\Delta_\mathrm{d}\approx 0.398$, since $\Delta_\mathrm{d}>\Omega_\mathrm{d}$ the transfer infidelity is still perfectly protected from the fluctuation of Doppler shift, arising a lower infidelity number $\sim 10^{-5}$ as compared to the $\chi=1$ case. Therefore, an enhanced sensitivity $\chi\geqslant 1$ enables the use of dressing fields far-detuned and achieves a higher-fidelity state transfer, thus staying a high-insensitivity to the inhomogeneous Doppler shift despite the continuous exposure of the atoms to the residual thermal motion. The potential application of this protection scheme to achieve robust Doppler-error erased gates have been profoundly discussed in the main text.

Appendix B. Other atomic temperature effects

In the main text, we show that our gates have a full insensitivity to the Doppler dephasing error induced by finite temperatures. However, during the gate execution, the residual thermal motion of atoms in the trap will also lead to other atomic temperature effects that affect the gate fidelity. Here, we consider the gate

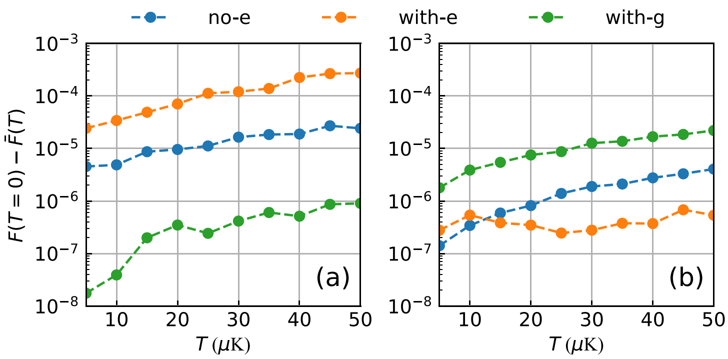

Figure 10. The gate infidelity $F(T=0)-\bar{F}(T)$ caused by (a) the fluctuated Rydberg interaction between two trapped atoms and (b) the inhomogeneous Rabi frequencies, both of which originate from the atomic thermal motion under a finite temperature T. Each point denotes the average of 300 realizations.

infidelity scales with the change of atomic position $\boldsymbol{r}$ [78], which satisfies a normal distribution

$$f(\boldsymbol{r})=\frac{1}{(2\pi)^{3/2}\,\sigma_x\sigma_y\sigma_z}\mathrm{e}^{-\frac{x^2}{2\sigma_x^2}}\mathrm{e}^{-\frac{y^2}{2\sigma_y^2}}\mathrm{e}^{-\frac{z^2}{2\sigma_z^2}} \tag{B1}$$

where $\boldsymbol{r}=\{x,y,z\}$ represents the real-time position. The standard deviation is $\sigma_{x,y,z}=\sqrt{k_{\mathrm{B}}T/m\omega_{x,y,z}^2}$ with T the temperature and $\omega_{x,y,z}$ the trapping frequency. We roughly estimate the maximal deviation of atomic position by $\sigma_{x,y,z}=(75,95,318)$ nm for trap frequencies $\omega_{x,y,z}=(147,117,35)$ kHz if $T=50\,\mu$K [67], while the real atomic position is randomly extracted from the distribution (B1) during each gate execution.

Fluctuation of Rydberg interaction. First of all, it is intuitive that the change in atomic position would result in a fluctuated Rydberg-Rydberg interaction, given by

$$V(\boldsymbol{r}_{12})=V_0+\delta V(\boldsymbol{r}_{12}-\boldsymbol{r}_0) \tag{B2}$$

where $\boldsymbol{r}_{12}=\boldsymbol{r}_1-\boldsymbol{r}_2$ is a relative distance of two atoms and $\boldsymbol{r}_1,\boldsymbol{r}_2$ are real atomic positions satisfying equation (B1) (note that $\boldsymbol{r}_0$ is the distance between two center of traps). The non-fluctuated interaction $V_0(r_0)=C_6/r_0^6$ is assumed with the *no-e* and *with-e* cases for a van der Waals shift; while for a resonant dipole–dipole interaction $V_0(r_0)=C_3/r_0^3$ corresponds to the *with-g* case. Here, the initial distance r_0 relative to the center of traps is calculated to be $r_0=|\boldsymbol{r}_0|\approx(4.03,3.41)\,\mu$m where the dispersion coefficients are $C_6/2\pi=863$ GHz.μm^6 and $C_3/2\pi=7.94$ GHz.μm^3 based on the choice of energy levels, respectively.

In addition, the change in Rydberg interaction can be described by

$$\begin{aligned}\delta V(\boldsymbol{r}_{12}-\boldsymbol{r}_0)&=-\frac{6C_6\,(\boldsymbol{r}_{12}-\boldsymbol{r}_0)}{r_0^7}\\ \delta V(\boldsymbol{r}_{12}-\boldsymbol{r}_0)&=-\frac{3C_3\,(\boldsymbol{r}_{12}-\boldsymbol{r}_0)}{r_0^4}\end{aligned} \tag{B3}$$

where $\boldsymbol{r}_{12}-\boldsymbol{r}_0$ means the realistic deviation to the relative distance of two atoms. During each realization j we could obtain a gate fidelity F_j with a random distance $\boldsymbol{r}_{12}$, and finally the average gate fidelity after sufficient realizations is provided by $\bar{F}(T)=\frac{1}{N}\sum_{j=1}^{N}F_j$ for a finite temperature T, where $N=300$ is used in the calculation.

As shown in figure 10(a), we calculate the infidelity $F(0)-\bar{F}(T)$ caused by the fluctuated Rydberg interaction. In general, the infidelity value keeps at a lower level $<10^{-3}$ for $T\leqslant 50\,\mu$K. In particular, it is worth noting that the *with-g* case benefits from the best infidelity as compared to other two cases, sustaining below 10^{-6}. Because the overall time-spent in the double Rydberg states $|ss\rangle$ and $|pp'\rangle$ is much shorter $P_{ss}+P_{pp'}\approx 8.885\times10^{-5}\,\mu$s, outperforming other cases ($P_{rr}\approx1.45\times10^{-4}$ for the *no-e* case and $P_{rr}\approx4.08\times10^{-4}$ for the *with-e* case) by almost 1 order of magnitude. In addition, we note that the interaction deviation caused by the dipole–dipole type $\delta V\propto 3C_3/r_0^4$ is relatively smaller than the van der Waals type $\delta V\propto 6C_6/r_0^7$ for each T, so as to provide a smaller impact on the gate performance.

Inhomogeneity of Rabi frequency. Next we also find that the uncertainty of atomic position would make the real laser amplitude perceived by atoms deviate from its desired value resulting in the position-dependent

Rabi frequency. To estimate this error, we replace the laser amplitudes $\Omega_\mathrm{r}(t)$ and $\Omega_\mathrm{r}'(t)$ by the position-dependent functions, as

$$\Omega_\mathrm{r}(t,\boldsymbol{r}) = \Omega_\mathrm{r}(t,0)\,\frac{\mathrm{e}^{-\frac{x^2}{\omega_{x,r}^2\left(1+z^2/L_{x,r}^2\right)}-\frac{y^2}{\omega_{y,r}^2\left(1+z^2/L_{y,r}^2\right)}}}{\left[\left(1+z^2/L_{x,r}^2\right)\left(1+z^2/L_{y,r}^2\right)\right]^{1/4}}$$

$$\Omega_\mathrm{r}'(t,\boldsymbol{r}') = \Omega_\mathrm{r}'(t,0)\,\frac{\mathrm{e}^{-\frac{x'^2}{\omega_{x,r}^2\left(1+z'^2/L_{x,r}^2\right)}-\frac{y'^2}{\omega_{y,r}^2\left(1+z'^2/L_{y,r}^2\right)}}}{\left[\left(1+z'^2/L_{x,r}^2\right)\left(1+z'^2/L_{y,r}^2\right)\right]^{1/4}}$$

where $\boldsymbol{r},\boldsymbol{r}'$ present the atomic position that satisfies the normal function (B1), and $\Omega_\mathrm{r}(t,0),\Omega_\mathrm{r}'(t,0)$ are the non-fluctuated pulse amplitudes same as $|\Omega_\mathrm{r}(t)|,|\Omega_\mathrm{r}'(t)|$ in equation (6). The laser beam waist is $\omega_{x(y),r}\approx 5.0\,\mu$m typically, arising the Rayleigh length $L_{x(y),r}\approx 62.93\,\mu$m for the effective two-photon wavelength $\lambda_\mathrm{eff}\approx 1248$ nm, when two lasers (780 nm and 480 nm) propagate in opposite directions. We observe that, even for $T = 50\,\mu$K the maximal position deviation of atoms is much smaller than the beam waist i.e. $\sigma_{x,y,z}\ll\omega_{x(y),r}$ which means the realistic deviation of Rabi frequency felt by atoms remains negligible. To verify this issue, we numerically calculate the infidelity caused by the inhomogeneity of Rabi frequencies in figure 10(b), with the variation of atomic temperature. As expected, the gate error contributes at a negligible level $10^{-7}\sim 10^{-5}$ for all cases, confirming the strong robustness of protocols to the deviation of atomic position.

ORCID iD

Jing Qian https://orcid.org/0000-0002-3085-8994

References

[1] Chao R and Reichardt B W 2018 Fault-tolerant quantum computation with few qubits *npj Quantum Inf.* **4** 42
[2] Cong I, Levine H, Keesling A, Bluvstein D, Wang S-T and Lukin M D 2022 Hardware-efficient, fault-tolerant quantum computation with Rydberg atoms *Phys. Rev. X* **12** 021049
[3] Chamberland C *et al* 2022 Building a fault-tolerant quantum computer using concatenated cat codes *PRX Quantum* **3** 010329
[4] Wu Y, Kolkowitz S, Puri S and Thompson J D 2022 Erasure conversion for fault-tolerant quantum computing in alkaline earth Rydberg atom arrays *Nat. Commun.* **13** 4657
[5] Ma S, Liu G, Peng P, Zhang B, Jandura S, Claes J, Burgers A P, Pupillo G, Puri S and Thompson J D 2023 High-fidelity gates and mid-circuit erasure conversion in an atomic qubit *Nature* **622** 279
[6] Scholl P, Shaw A L, Tsai R B-S, Finkelstein R, Choi J and Endres M 2023 Erasure conversion in a high-fidelity Rydberg quantum simulator *Nature* **622** 273
[7] Vasilev G S, Kuhn A and Vitanov N V 2009 Optimum pulse shapes for stimulated raman adiabatic passage *Phys. Rev. A* **80** 013417
[8] Pagano A, Weber S, Jaschke D, Pfau T, Meinert F, Montangero S and Büchler H P 2022 Error budgeting for a controlled-phase gate with strontium-88 Rydberg atoms *Phys. Rev. Res.* **4** 033019
[9] Evered S J *et al* 2023 High-fidelity parallel entangling gates on a neutral-atom quantum computer *Nature* **622** 268
[10] Mohan M, de Keijzer R and Kokkelmans S 2023 Robust control and optimal Rydberg states for neutral atom two-qubit gates *Phys. Rev. Res.* **5** 033052
[11] Chang T H, Wang T N, Jen H H and Chen Y-C 2023 High-fidelity Rydberg controlled-z gates with optimized pulses *New J. Phys.* **25** 123007
[12] Goerz M H, Halperin E J, Aytac J M, Koch C P and Whaley K B 2014 Robustness of high-fidelity Rydberg gates with single-site addressability *Phys. Rev. A* **90** 032329
[13] Güngördü U and Kestner J P 2022 Robust quantum gates using smooth pulses and physics-informed neural networks *Phys. Rev. Res.* **4** 023155
[14] Jandura S, Thompson J D and Pupillo G 2023 Optimizing Rydberg gates for logical-qubit performance *PRX Quantum* **4** 020336
[15] Poggi P M, De Chiara G, Campbell S and Kiely A 2024 Universally robust quantum control *Phys. Rev. Lett.* **132** 193801
[16] Zhang C, Liu Y, Song J, Xia Y and Shi Z-C 2024 High-fidelity quantum gates via optimizing short pulse sequences in three-level systems *New J. Phys.* **26** 013024
[17] Shi Z-C, Ding J-T, Chen Y-H, Song J, Xia Y, Yi X and Nori F 2024 Supervised learning for robust quantum control in composite-pulse systems *Phys. Rev. Appl.* **21** 044012
[18] Fromonteil C, Bluvstein D and Pichler H 2023 Protocols for Rydberg entangling gates featuring robustness against quasistatic errors *PRX Quantum* **4** 020335
[19] Fu Z *et al* 2022 High-fidelity entanglement of neutral atoms via a Rydberg-mediated single-modulated-pulse controlled-phase gate *Phys. Rev. A* **105** 042430
[20] Graham T M, Kwon M, Grinkemeyer B, Marra Z, Jiang X, Lichtman M T, Sun Y, Ebert M and Saffman M 2019 Rydberg-mediated entanglement in a two-dimensional neutral atom qubit array *Phys. Rev. Lett.* **123** 230501
[21] Wilk T, Gaëtan A, Evellin C, Wolters J, Miroshnychenko Y, Grangier P and Browaeys A 2010 Entanglement of two individual neutral atoms using Rydberg blockade *Phys. Rev. Lett.* **104** 010502
[22] Isenhower L, Urban E, Zhang X L, Gill A T, Henage T, Johnson T A, Walker T G and Saffman M 2010 Demonstration of a neutral atom controlled-not quantum gate *Phys. Rev. Lett.* **104** 010503

[23] Zeng Y, Xu P, He X, Liu Y, Liu M, Wang J, Papoular D J, Shlyapnikov G V and Zhan M 2017 Entangling two individual atoms of different isotopes via Rydberg blockade *Phys. Rev. Lett.* **119** 160502
[24] Levine H *et al* 2019 Parallel implementation of high-fidelity multiqubit gates with neutral atoms *Phys. Rev. Lett.* **123** 170503
[25] McDonnell K, Keary L F and Pritchard J D 2022 Demonstration of a quantum gate using electromagnetically induced transparency *Phys. Rev. Lett.* **129** 200501
[26] Ryabtsev I I, Beterov I I, Tretyakov D B, Entin V M and Yakshina E A 2011 Doppler- and recoil-free laser excitation of Rydberg states via three-photon transitions *Phys. Rev. A* **84** 053409
[27] Kaufman A M, Lester B J and Regal C A 2012 Cooling a single atom in an optical tweezer to its quantum ground state *Phys. Rev. X* **2** 041014
[28] Thompson J D, Tiecke T G, Zibrov A S, Vuletić V and Lukin M D 2013 Coherence and raman sideband cooling of a single atom in an optical tweezer *Phys. Rev. Lett.* **110** 133001
[29] Finkelstein R, Lahad O, Cohen I, Davidson O, Kiriati S, Poem E and Firstenberg O 2021 Continuous protection of a collective state from inhomogeneous dephasing *Phys. Rev. X* **11** 011008
[30] Davidson O, Yogev O, Poem E and Firstenberg O 2023 Fast, noise-free atomic optical memory with 35-percent end-to-end efficiency *Commun. Phys.* **6** 131
[31] Sun Y, Xu P, Chen P-X and Liu L 2020 Controlled phase gate protocol for neutral atoms via off-resonant modulated driving *Phys. Rev. Appl.* **13** 024059
[32] Jandura S and Pupillo G 2022 Time-Optimal Two- and Three-Qubit Gates for Rydberg Atoms *Quantum* **6** 712
[33] Song P-Y, Wei J-F, Xu P, Yan L-L, Feng M, Su S-L and Chen G 2024 Fast realization of high-fidelity nonadiabatic holonomic quantum gates with a time-optimal-control technique in Rydberg atoms *Phys. Rev. A* **109** 022613
[34] Saffman M, Beterov I I, Dalal A, Páez E J and Sanders B C 2020 Symmetric Rydberg controlled-*z* gates with adiabatic pulses *Phys. Rev. A* **101** 062309
[35] Cesa F and Pichler H 2023 Universal quantum computation in globally driven Rydberg atom arrays *Phys. Rev. Lett.* **131** 170601
[36] Shi X-F 2018 Accurate quantum logic gates by spin echo in Rydberg atoms *Phys. Rev. Appl.* **10** 034006
[37] Thoumany P, Hänsch T, Stania G, Urbonas L and Becker T 2009 Optical spectroscopy of rubidium Rydberg atoms with a 297 nm frequency-doubled dye laser *Opt. Lett.* **34** 1621
[38] Urban E, Johnson T A, Henage T, Isenhower L, Yavuz D D, Walker T G and Saffman M 2009 Observation of Rydberg blockade between two atoms *Nat. Phys.* **5** 110
[39] Gaëtan A, Miroshnychenko Y, Wilk T, Chotia A, Viteau M, Comparat D, Pillet P, Browaeys A and Grangier P 2009 Observation of collective excitation of two individual atoms in the Rydberg blockade regime *Nat. Phys.* **5** 115
[40] Müller M M, Reich D M, Murphy M, Yuan H, Vala J, Whaley K B, Calarco T and Koch C P 2011 Optimizing entangling quantum gates for physical systems *Phys. Rev. A* **84** 042315
[41] Müller M M, Said R S, Jelezko F, Calarco T and Montangero S 2022 One decade of quantum optimal control in the chopped random basis *Rep. Prog. Phys.* **85** 076001
[42] Li S X, Mu W L, You J B and Shao X Q 2024 Simulation of a feedback-based algorithm for quantum optimization for a realistic neutral-atom system with an optimized small-angle controlled-phase gate *Phys. Rev. A* **109** 062603
[43] Li R, Li S, Yu D, Qian J and Zhang W 2022 Optimal model for fewer-qubit cnot gates with Rydberg atoms *Phys. Rev. Appl.* **17** 024014
[44] Braaten E, Hammer H-W and Lepage G P 2017 Lindblad equation for the inelastic loss of ultracold atoms *Phys. Rev. A* **95** 012708
[45] Sun L-N, Yan L-L, Su S-L and Jia Y 2021 One-step implementation of time-optimal-control three-qubit nonadiabatic holonomic controlled gates in Rydberg atoms *Phys. Rev. Appl.* **16** 064040
[46] Li R, Qian J and Zhang W 2023 Proposal for practical Rydberg quantum gates using a native two-photon excitation *Quantum Sci. Technol.* **8** 035032
[47] Shi X-F 2020 Transition slow-down by Rydberg interaction of neutral atoms and a fast controlled-not quantum gate *Phys. Rev. Appl.* **14** 054058
[48] Keating T, Cook R L, Hankin A M, Jau Y-Y, Biedermann G W and Deutsch I H 2015 Robust quantum logic in neutral atoms via adiabatic Rydberg dressing *Phys. Rev. A* **91** 012337
[49] Shi X-F 2020 Suppressing motional dephasing of ground-Rydberg transition for high-fidelity quantum control with neutral atoms *Phys. Rev. Appl.* **13** 024008
[50] de Léséleuc S, Barredo D, Lienhard V, Browaeys A and Lahaye T 2018 Analysis of imperfections in the coherent optical excitation of single atoms to Rydberg states *Phys. Rev. A* **97** 053803
[51] Li X, Shao X and Li W 2022 Single temporal-pulse-modulated parameterized controlled-phase gate for Rydberg atoms *Phys. Rev. Appl.* **18** 044042
[52] Maxwell D, Szwer D J, Paredes-Barato D, Busche H, Pritchard J D, Gauguet A, Weatherill K J, Jones M P A and Adams C S 2013 Storage and control of optical photons using Rydberg polaritons *Phys. Rev. Lett.* **110** 103001
[53] Dudin Y O and Kuzmich A 2012 Strongly interacting Rydberg excitations of a cold atomic gas *Science* **336** 887
[54] Beterov I I and Saffman M 2015 Rydberg blockade, förster resonances and quantum state measurements with different atomic species *Phys. Rev. A* **92** 042710
[55] Maller K M, Lichtman M T, Xia T, Sun Y, Piotrowicz M J, Carr A W, Isenhower L and Saffman M 2015 Rydberg-blockade controlled-not gate and entanglement in a two-dimensional array of neutral-atom qubits *Phys. Rev. A* **92** 022336
[56] Zhang X L, Gill A T, Isenhower L, Walker T G and Saffman M 2012 Fidelity of a Rydberg-blockade quantum gate from simulated quantum process tomography *Phys. Rev. A* **85** 042310
[57] Kinos A and Mølmer K 2023 Optical multiqubit gate operations on an excitation-blockaded atomic quantum register *Phys. Rev. Res.* **5** 013205
[58] Mitra A, Martin M J, Biedermann G W, Marino A M, Poggi P M and Deutsch I H 2020 Robust mlmer-srensen gate for neutral atoms using rapid adiabatic Rydberg dressing *Phys. Rev. A* **101** 030301
[59] Jiang X, Scott J, Friesen M and Saffman M 2023 Sensitivity of quantum gate fidelity to laser phase and intensity noise *Phys. Rev. A* **107** 042611
[60] He C and Jones R R 2024 Active suppression of quantum dephasing in resonantly driven ensembles *Phys. Rev. Lett.* **132** 043201
[61] Hou Q-L, Wang H and Qian J 2024 Active robustness against detuning error for Rydberg quantum gates *Phys. Rev. Appl.* **22** 034054
[62] Ravets S, Labuhn H, Barredo D, Béguin L, Lahaye T and Browaeys A 2014 Coherent dipole–dipole coupling between two single Rydberg atoms at an electrically-tuned förster resonance *Nat. Phys.* **10** 914
[63] Beterov I I, Saffman M, Yakshina E A, Tretyakov D B, Entin V M, Bergamini S, Kuznetsova E A and Ryabtsev I I 2016 Two-qubit gates using adiabatic passage of the stark-tuned förster resonances in Rydberg atoms *Phys. Rev. A* **94** 062307

[64] Petrosyan D, Motzoi F, Saffman M and Mølmer K 2017 High-fidelity Rydberg quantum gate via a two-atom dark state *Phys. Rev. A* **96** 042306
[65] Li B, Li M, Jiang X, Qian J, Li X, Liu L and Wang Y 2019 Optical spectroscopy of *np* Rydberg states of ^{87}Rb atoms with a 297-nm ultraviolet laser *Phys. Rev. A* **99** 042502
[66] Urvoy A, Ripka F, Lesanovsky I, Booth D, Shaffer J P, Pfau T and Löw R 2015 Strongly correlated growth of Rydberg aggregates in a vapor cell *Phys. Rev. Lett.* **114** 203002
[67] Chew Y, Tomita T, Mahesh T P, Sugawa S, de Léséleuc S and Ohmori K 2022 Ultrafast energy exchange between two single Rydberg atoms on a nanosecond timescale *Nat. Photon.* **16** 724
[68] Ripka F, Kübler H, Löw R and Pfau T 2018 A room-temperature single-photon source based on strongly interacting Rydberg atoms *Science* **362** 446
[69] Yang B, Sun H, Huang C-J, Wang H-Y, Deng Y, Dai H-N, Yuan Z-S and Pan J-W 2020 Cooling and entangling ultracold atoms in optical lattices *Science* **369** 550
[70] Lorenz N, Festa L, Steinert L-M and Gross C 2021 Raman sideband cooling in optical tweezer arrays for Rydberg dressing *SciPost Phys.* **10** 052
[71] Cooper A, Covey J P, Madjarov I S, Porsev S G, Safronova M S and Endres M 2018 Alkaline-earth atoms in optical tweezers *Phys. Rev. X* **8** 041055
[72] Ai M-Z, Li S, Hou Z, He R, Qian Z-H, Xue Z-Y, Cui J-M, Huang Y-F, Li C-F and Guo G-C 2020 Experimental realization of nonadiabatic holonomic single-qubit quantum gates with optimal control in a trapped ion *Phys. Rev. Appl.* **14** 054062
[73] Saffman M and Walker T G 2005 Analysis of a quantum logic device based on dipole-dipole interactions of optically trapped Rydberg atoms *Phys. Rev. A* **72** 022347
[74] Tamura H, Yamakoshi T and Nakagawa K 2020 Analysis of coherent dynamics of a Rydberg-atom quantum simulator *Phys. Rev. A* **101** 043421
[75] Müller M M, Murphy M, Montangero S, Calarco T, Grangier P and Browaeys A 2014 Implementation of an experimentally feasible controlled-phase gate on two blockaded Rydberg atoms *Phys. Rev. A* **89** 032334
[76] Levine H, Keesling A, Omran A, Bernien H, Schwartz S, Zibrov A S, Endres M, Greiner M, Vuletić V and Lukin M D 2018 High-fidelity control and entanglement of Rydberg-atom qubits *Phys. Rev. Lett.* **121** 123603
[77] Blanes S, Casas F, Oteo J and Ros J 2009 The magnus expansion and some of its applications *Phys. Rep.* **470** 151
[78] Robicheaux F, Graham T M and Saffman M 2021 Photon-recoil and laser-focusing limits to Rydberg gate fidelity *Phys. Rev. A* **103** 022424